Author/s:
Mazumder, A;Ahmed, T;Mayes, E;Tawfik, SA;Russo, SP;Low, MX;Ranjan, A;Balendhran, S;Walia, S

Title:
Nonvolatile Resistive Switching in Layered InSe via Electrochemical Cation Diffusion

Date:
2022-04-01

Citation:
Mazumder, A., Ahmed, T., Mayes, E., Tawfik, S. A., Russo, S. P., Low, M. X., Ranjan, A., Balendhran, S. & Walia, S. (2022). Nonvolatile Resistive Switching in Layered InSe via Electrochemical Cation Diffusion. Advanced Electronic Materials, 8 (4), https://doi.org/10.1002/aelm.202100999.

Non-volatile resistive switching in layered InSe via electrochemical cation diffusion

Aishani Mazumder [1,†], Taimur Ahmed [1,2,3,†,], Edwin Mayes[4], Sherif Abdulkader Tawfik[5,6], Salvy P. Russo[6,7], Mei Xian Low[1,2], Abhishek Ranjan[8], Sivacarendran Balendhran[9], Sumeet Walia [1,2*]*

[1] School of Engineering, RMIT University, 124 La Trobe Street, Melbourne 3000, Australia

[2]Functional Materials and Microsystems Research Group and the Micro Nano Research Facility, RMIT University, Melbourne 3000, Australia

[3]Pak-Austria Fachhochschule: Institute of Applied Sciences and Technology, Haripur 22620, Pakistan

[4]School of Science, RMIT University, 124 La Trobe Street, Melbourne 3000, Australia

[5]Institute for Frontier Materials, Deakin University, Geelong 3216, Australia

[6]ARC Centre of Excellence in Exciton Science, School of Science, RMIT University, Melbourne 3000, Australia

[7]Chemical and Quantum Physics, School of Science, RMIT University, Melbourne 3000, Australia

This is the author manuscript accepted for publication and has undergone full peer review but has not been through the copyediting, typesetting, pagination and proofreading process, which may lead to differences between this version and the Version of Record. Please cite this article as doi: 10.1002/aelm.202100999.

[8]School of Engineering, Sapienza University of Rome, Piazzale Aldo Moro, 5, 00185 Roma, Italy

[9]School of Physics, Melbourne University, The University of Melbourne, Parkville 3010, Australia

*Correspondence to: Dr. Taimur Ahmed, Associate Professor Sumeet Walia

E-mail: taimurahmad1@gmail.com, sumeet.walia@rmit.edu.au

[†] These authors contributed equally.

Keywords: layered InSe, non-volatile resistive switching, memory, two-dimensional, silver cation, nanofilament

Abstract

Two-dimensional (2D) materials are increasingly being investigated for their non-volatile switching properties as a step towards downscaling of core electronics elements. Here, we investigate the interplay between electrochemically active silver (Ag) cations and layered Indium selenide (InSe), a 2D metal monochalcogenide, to demonstrate a non-volatile switching device. Detailed microscopic characterisation supported with Density Functional Theory (DFT) calculations reveal cationic filamentary based non-volatile switching mechanism of γ-InSe in a cross-planar architecture. This is electrically driven by diffusion of Ag ions through the layered InSe stack. The InSe based memory

cells exhibit a switching ratio of ~ 10^3 and a memory retention of > 10^5 seconds. This work opens new opportunities to enhance resistive switching performances of 2D materials for next generation information storage and brain inspired computation using active metal diffusion.

Introduction

While miniaturization of devices continues for new and emerging applications, the increasing demand for memory capacity will soon bring silicon-based memory technology to its critical physical limit. In this context, resistive random-access memories have demonstrated significant promise owing to their scalability, low-energy consumption, compatibility with existing complementary metal oxide semiconductor (CMOS) processes and the exciting potential in neuromorphic computing.[1-6] *Moreover, their ability to perform multi-level cell (MLC) operation render them a viable choice for next generation neuromorphic electronics.*[7] The development of 2D materials particularly over the past decade presents new opportunities as they provide an atomically flat[8] surface potentially free from surface dangling bonds.[9] This provides several advantages in suppressing leakage-currents and increased mechanical flexibility.[8]

Recently, 2D transition-metal dichalcogenides,[10] transition-metal oxide (such as MoO_3),[8] hexagonal boron nitride (*h*-BN) [11] and elemental black phosphorus (BP)[12] have been used in vertically stacked resistive memory devices. These results are significant, however there remain quite a few areas that need further investigation in the domain of 2D materials based resistive memory technologies.[5, 8, 11-15] These include investigations into charge transport mechanisms in vertically stacked van der Waals

structures and understanding the role of energy barrier of the van der Waals layers to the out-of-plane cationic and anionic diffusion.

Layered InSe is a relatively recently investigated semiconductor from the post transition metal chalcogenide family.[16] Often, characterised by a relatively slow ambient oxidation[17] unlike other 2D materials such as molybdenum di-sulphide (MoS_2)[18] and BP.[17] Recently, oxidized InSe has been reported to demonstrate a current hysteresis,[19] which indicates its viability for memory applications. With a reported dark current in the sub nano ampere range,[20-21] layered InSe can be used to realise energy-efficient memristors with high integration density.[5] It has been previously shown that introduction of silver (Ag) in indium based compounds result in the formation of cationic interstitial sites and that Ag substitutes *indium*, resulting in cationic vacancies.[22] The mobility of *indium* ion in an InSe matrix can thereby allow controllable migration of electrochemically active ions to migrate across InSe thereby allowing for cationic driven memristive applications. *The use of Ag as an electrochemically active electrode material here can be owed to the feasibility of Ag electrode for fast redox reactions and high mobility for electrochemical metallization (ECM) based memory cells.[23] Electrodes with lower cationic mobility and slower redox reactions can lead to migration congestion or low cluster formation thereby hindering filamentary growth.[24] This in turn makes Ag filament based ECM memory a sought after option for resistive switching in non-volatile memory systems.[25]* Herein, we demonstrate the mechanism of Ag diffusion in InSe and formation of a cationic filament enabling the non-volatile resistive switching behaviour in InSe with switching ratios of 10^3 and prolonged memory retention of 10^4 - 10^5 seconds. *The large switching window observed in the memory cells can be used to develop multi-level memory applications by controlling the current compliance to generate mid-resistive states, similar to shown in other electrically driven Re-RAM devices.[26-27] Moreover, the photodetection capabilities of InSe[21, 28-30] can render it feasible*

for future applications in multi-state non-volatile opto-electronic resistive memory, as previously reported in other 2D materials.[31] To investigate the switching mechanism, detailed microscopic characterisations *and theoretical calculations* are used to postulate a mechanism of Ag diffusion driven switching. Thereby, opening a new pathway to create memory devices based on a multitude of 2D material systems.

Results and Discussions

Micromechanically exfoliated InSe flakes were sandwiched between Ag (bottom) and chrome/gold (Cr/Au) (top) electrodes in a cross-planar architecture, using a manual transfer stage (see Methods section for further details). **Figure 1a** shows an optical microscopic photograph of a representative InSe cross-point memory cell fabricated on a silicon dioxide (SiO_2)/silicon (Si) substrate. The memory device operates on a vertical charge transfer mechanism, which occurs in the cross-point active device area of $> 5\ \mu m^2$, between Ag and Cr/Au electrodes. Figure 1b shows the atomic force microscope (AFM) topographic scan obtained for the representative device before the fabrication of top electrode. A thickness of 8.8 nm was measured as indicated in the thickness profile in Figure 1c. See Section 1 (Figure S1) of Supplementary Information for optical images of cross-planar InSe devices before and after deposition of top electrode and their respective AFM profiles.

To investigate the crystallographic structure, the lattice spacing of the switching medium and the interfaces of the stack, a lamella is cut-out from an as-fabricated device and used for cross-sectional transmission electron microscope (TEM) imaging (see Methods). Figure S2 in Supplementary Information shows scanning electron microscope (SEM) image of a pristine

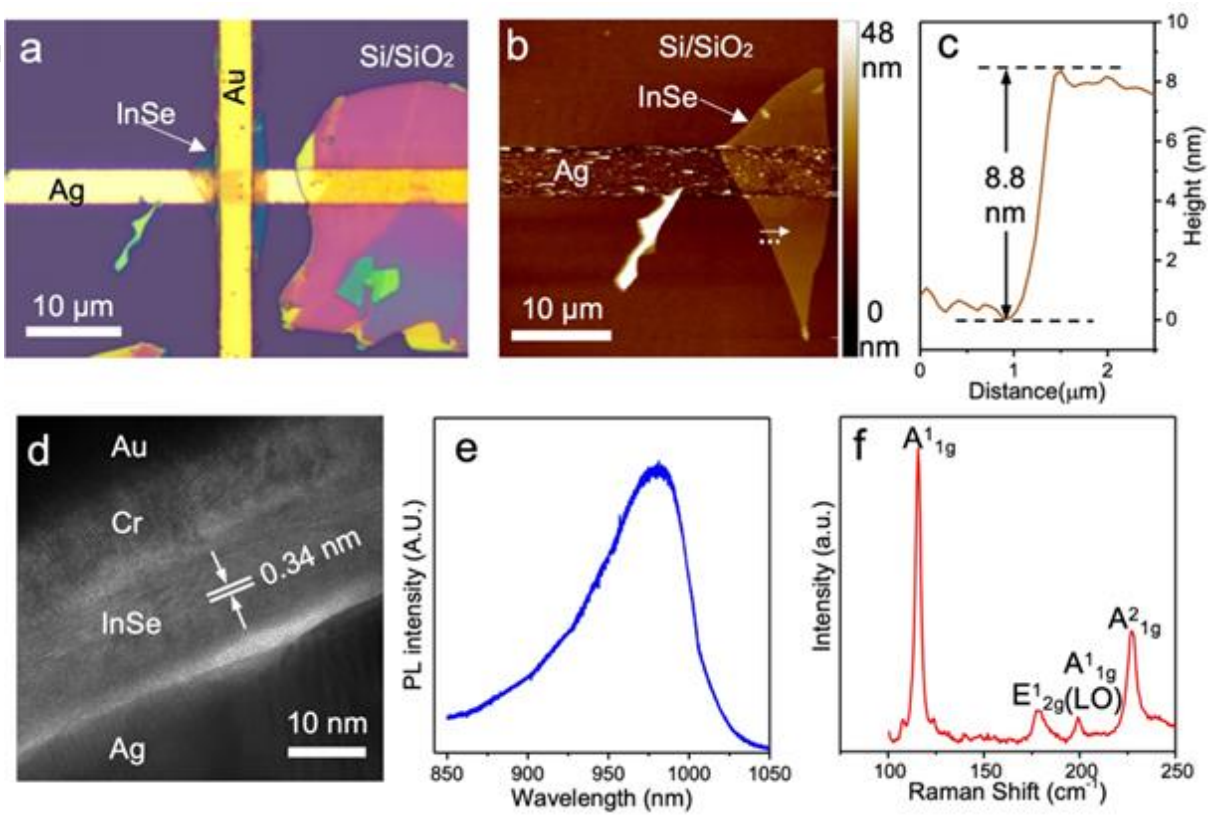

Figure 1: Structural, microscopic and spectroscopic characterisation of an InSe memory cell. (a) Optical image of a representative cross-point InSe memory device with Ag as bottom and Au as top electrode. (b) AFM topographic image of a mechanically exfoliated flake transferred onto Ag electrode. (c) AFM height profile of the InSe flake shown in (b). (d) Cross-sectional HRTEM image of a pristine InSe memory device. (e) Photoluminescence spectrum of a bulk InSe flake. (f) Raman spectrum of the exfoliated multilayer γ-InSe flake.

cross-point memory device used for lamella preparation. A high-resolution transmission electron microscope (HRTEM) image is shown in Figure 1d, where the layered structure of InSe can be clearly seen between top and bottom electrodes. For multilayer InSe, a varying interlayer distance in the range of 0.24-0.34 nm has been previously reported in literature.[32] A line profile across our InSe stack shows a *d*-spacing of 0.34 nm (Supplementary Information Section 1, Figure S2).

For further analysis, photoluminescence (PL) and Raman characterisations are performed. The PL spectrum of the micromechanically exfoliated InSe is shown in Figure 1e. An emission peak centred at 980 nm is seen, corresponding to the bandgap value of 1.26 eV for InSe.[33-34] Raman spectral analysis is performed on the InSe layers to further characterise its composition and crystalline phase. The Raman spectrum collected from the flake used in the memory device (Figure 1f**)** indicates γ-phase of InSe. The signature Raman modes A^1_{1g} (115.1 cm^{-1}), E^1_{2g} (177.8 cm^{-1}), A^1_{1g} (LO at 199.5 cm^{-1}) and A^2_{1g} (226.7 cm^{-1}) can be associated with the γ-phase.[34-35] A spectral intensity map of the A^1_{1g} Raman peak is used to characterize the active area for charge transport in the device, which is shown in Supplementary Information, Figure S2.

Figure 2a schematically illustrates the device structure and the electrical biasing scheme for memory operations. *Cross-point memory devices with 10-30 InSe mono-layers (8.8-25 nm) were characterized for their non-volatile switching behaviour*.[36] The bottom Ag electrode of the device is subjected to a variable voltage and the top electrode is grounded. The pristine InSe memory cells exhibit high resistance in the range of megaohms, indicating highly resistive out of plane conduction in pristine InSe flakes. The memory cells are subjected to a positively biased electroforming voltage at the bottom Ag electrode which results in a high jump in conductance (shown in Supplementary Information Figure S3). Figure 2b shows post-electroforming current-voltage characteristics which

displays a bipolar non-volatile switching behaviour. The bipolar switching characteristics of our InSe memory devices can be attributed to the redox processes at the bottom Ag electrode enabling the migration of silver (Ag^+) cations in the InSe matrix which is discussed later in the paper.[37-38] A positive bias applied on the bottom Ag electrode sets the device to a low resistive state (LRS) whereas a negative bias sets our memory cell to a high resistive state (HRS), as indicated in Figure 2b. *Upon the application of a positive SET bias of +2V, the device switches from a HRS state to LRS state and retains its state. On the other hand, -2V is applied to RESET the device where, upon the application of negative polarity the device goes from LRS state to HRS state and maintains its state. The physical mechanism of this non-volatile switching in the InSe memory cell is discussed in detail later in this section.* Figure 2c demonstrates the statistical distribution for the SET and RESET voltages for the devices. A median SET voltage (V_{SET}) of 0.95 V and RESET voltage (V_{RESET}) of -0.67 V are measured during cyclic resistive switching. These voltage values can be regarded as the voltages required to change the conductance state of the memory cell.[39] As observed from the HRS/LRS retention plot in Figure 2d, the memory cell sustained its resistive states for more than 24 hours, measured under a constant read voltage (V_{READ}) of 0.2 V at ambient conditions. *For this memory retention measurement, the LRS and HRS states were attained by applying a SET and RESET bias of 2V and -2V, respectively. A* switching ratio of ~ 10^3 (HRS:LRS) is observed without any obvious decline over the given time period. Furthermore, cyclic endurance of the device is shown in Figure 2e. The memory cell retains its switching for around 50 cycles. However, there is a decrease in resistance in the HRS state which can be due to the formation of some permanent filamentary pathways. To reveal the role of the electrode material in the switching mechanism, Au/InSe/Cr/Au devices were fabricated (see Supplementary Information Figure *S4*). The Au/InSe/Cr/Au device exhibited lower

switching ratio of ~10^1 and a poor retention of its LRS state (<500 seconds). The *very small* switching window can be associated with partial diffusion

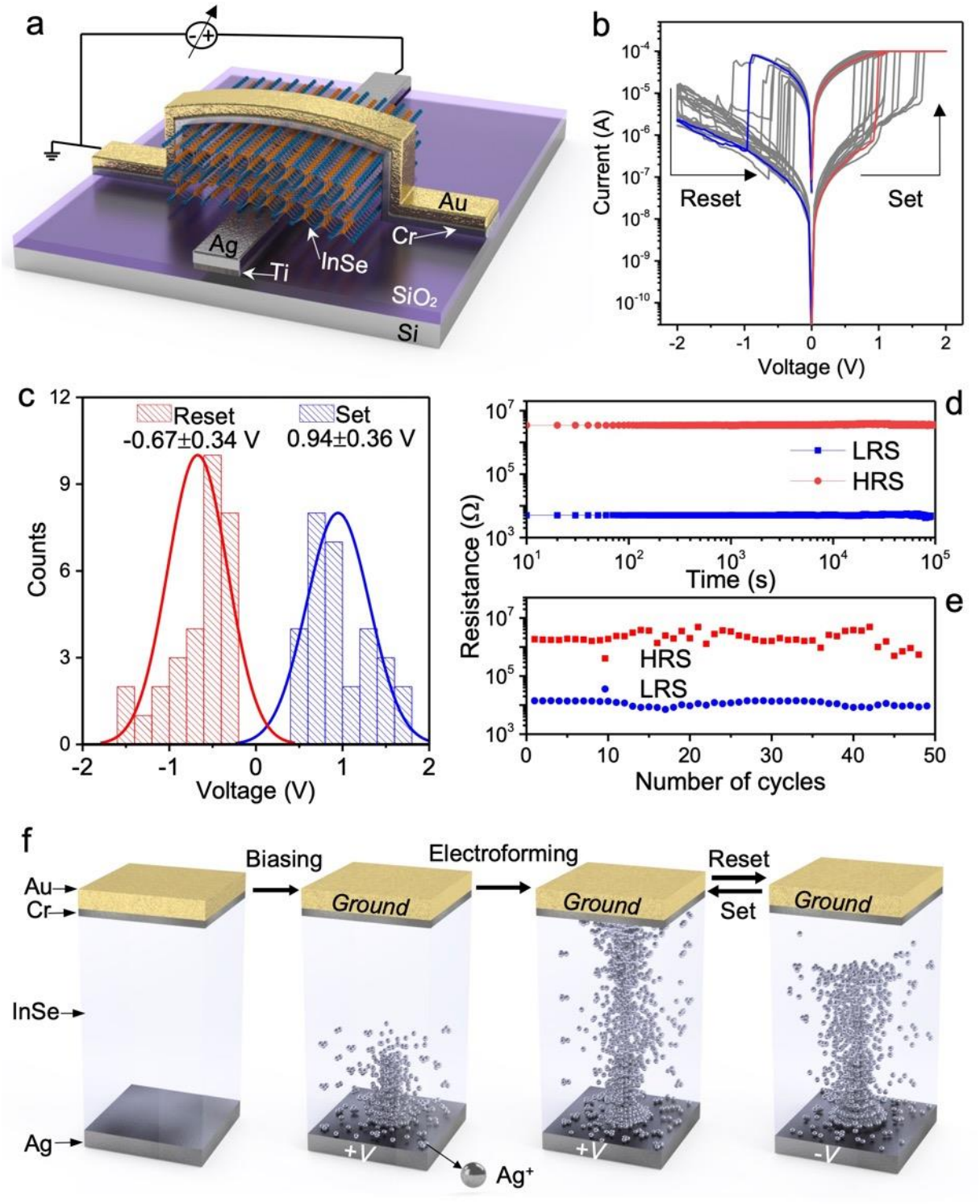

Figure 2: Electrical characterisation and mechanism of charge transfer in InSe memory cell (a) cross-sectional schematic of the InSe memory device. (b) *I-V* characteristics of the memory cell in ambient conditions *under multiple voltage sweeps between +2 V to SET and -2 V to RESET the device.* (c) Statistical analysis of SET threshold voltage (d) Statistical analysis of RESET threshold voltage. (e) Time dependent HRS and LRS retention characteristics for 10^5 s. (f) Cyclic endurance of the InSe memory cell. (g) bipolar non-volatile switching mechanism of the memory cell.

of oxygen species[4] from Cr which has a larger diffusion barrier relative to Ag (discussed later). To further understand the role of the electrode, Au/InSe/Au devices were subjected to an electroforming bias which resulted in the device to undergo an irreversible hard breakdown *(Supplementary Information Figure S4).* We did not observe the substantial non-volatile switching characteristics in devices without the Ag electrode *(Section 4 of Supplementary Information).* Based on the bipolar switching characteristics of our InSe memory devices, we propose that the switching mechanism is underpinned by the migration of Ag^+ ions.

As observed from the double-logarithmically *I-V* plot (Supplementary Information Figure *S4*), the device exhibits a Schottky behaviour in the HRS state whereas an Ohmic trend in the LRS state. The rectifying characteristic can be attributed to the formation of Schottky contact between InSe and *Cr* interface.[40] The switching phenomenon is in accordance with the space charge limited conduction (SCLC) mechanism[41] and can be attributed to the ionization of electrode material and injection of charges from the electrodes into the switching media. As such, we observe a sequence of a trap free SCLC behaviour ($I \propto V^4$) in the HRS state, followed by observation of Childs

law ($I \propto V^2$) and then ohmic conduction ($I \propto V$) in the LRS state.[41] Based on the interpretation of the electrical data a model of the possible switching mechanism was developed as depicted in Figure 2f. When a positive bias is applied on the bottom electrode, Ag starts to oxidise to form Ag^+ ions, which are then injected into the InSe. *It is well established that, InSe can form a number of vacancies on the top surface and the edges of the exfoliated flakes when exposed to ambient conditions.[17-18, 42-46] As a result of our fabrication process of micromechanical exfoliation and transfer technique these vacancies are expected to be present near the top and bottom electrode interfaces and the cleaved surfaces of the flake.* Subsequently, *these* Ag ions take up the path of shortest resistance at bottom electrode interfaces through *the* vacancies to move towards the top electrode.[42] *Alongside vacancy intermediated diffusion of Ag at electrode interfaces, migration of Ag can also be possible by the creation of indium interstitials.[47] To eliminate the possibility of formation of an Ag-In-Se precipitate our Bader charge analysis reveal the electron charges of indium, selenium and Ag to be +0.6 |e|, -0.6|e|, +0.2|e| respectively. This indicates the replacement of a single Ag ion in the cationic vacancy is thermodynamically unfavourable thereby, eliminating the possibility of precipitate formation and indicating presence of mobile Ag^+ in the stack for resistive switching purposes.* With increasing electric field strength, a larger number of *these mobile* cations are generated from the bottom electrode, which then diffuse toward the top electrode to form the conductive pathway.[48] This in turn SETs the device to a high conductive state (*i.e.*, LRS state). Upon the reversal of the polarity of the applied bias, the silver ions are repelled from the top electrode fragmenting the formed conductive filament, resulting in the resetting of the device to the HRS. This bipolar switching mechanism enables the device to act as a non-volatile memory cell for storing and erasing data with the SET and RESET processes, respectively.

The migration of silver ions into InSe for non-volatile switching is confirmed from the structural and microscopic characterization and further supported by theoretical modelling using DFT. First, to underpin the switching mechanism and experimentally observe the migration of Ag ions through InSe layer, a comparative cross-sectional TEM analysis between the pristine and electroformed devices was conducted. *The STEM images show the two separate lamellae's* obtained from a pristine InSe device (**Figure 3a**) and an electroformed device (Figure 3b), which were then subjected to Energy-dispersive X-ray spectroscopy (EDX) scan. The EDX line scans across both the pristine and electroformed InSe memory cells (Figure 3c and 3d, respectively) indicate the presence of an oxide layer at the InSe/Ag electrode interfaces. This can be attributed to the oxidation of InSe and/or silver under ambient conditions

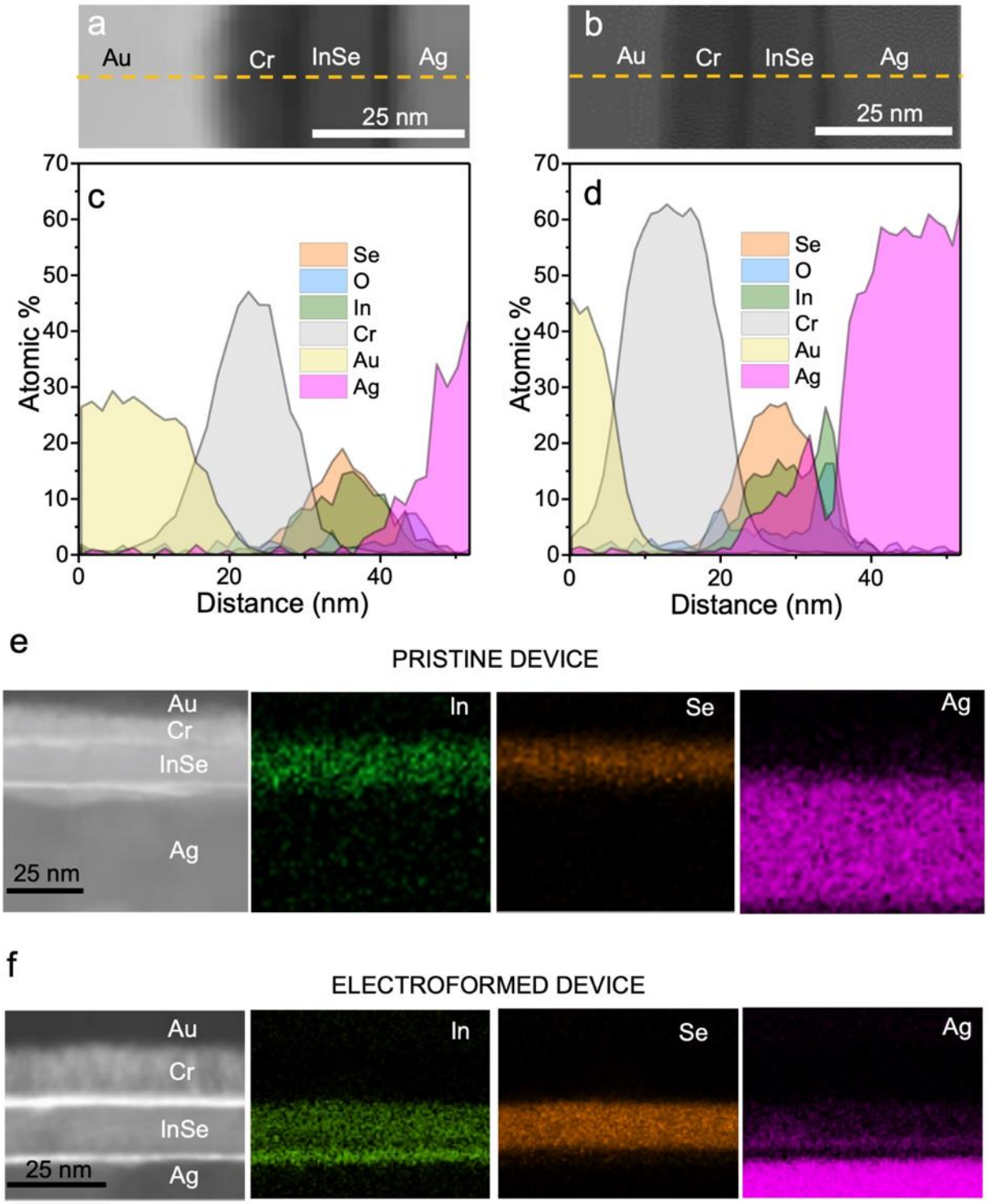

Figure 3: Microscopic analysis of InSe memory cell. Cross-sectional STEM images of (a) pristine and (b) electroformed InSe memory device. The corresponding EDX profile scans of (c) pristine and

(d) electroformed InSe stack. EDX maps and STEM image of (e) pristine and (f) electroformed InSe lamellae, indicating the elemental distribution of In, Se and Ag across the stack.

or during device fabrication, resulting in a thin amorphous native oxide layer. [49-50] The indium/selenium ratio of unity is measured in the pristine device whereas a decrease in the indium concentration with an accumulation of indium at the bottom electrode interface is observed in the electroformed InSe device. *Despite being cationic in nature, the accumulation of the indium ions at the bottom interface in Figure 3d is possibly a result of the application of a RESET polarity before the lamella preparation. However, the existence of cationic silver in the stack upon the application of the same RESET polarity can be attributed to the formation of semi-permanent filamentary pathways, as seen previously in literature.*[1] Upon the *application of positive bias,* the Ag ions tend migrate towards the top electrode, which they do by occupying interstitial sites created by *indium*, as well as pushing *indium* ions out to occupy the position. The smaller ionic radius of silver as compared to indium also allows for it to easily occupy the vacant sites. The comparative study of the EDX maps of the pristine (Figure 3e) and electroformed device (Figure 3f) reveal an influx of Ag in the InSe layer after *cyclic switching,* similar to those of the line scans seen in Figure 3c and d. This confirms our proposed hypothesis of silver migration for non-volatile switching in InSe. This mechanism is similar to the formation of conduction pathway for non-volatile switching in 2D materials, that have been reported previously.[11, 51] Based on the results, it can be inferred that the application of positive bias in our memory cell facilitates the generation and diffusion of Ag^+ ions towards the top Cr/Au electrode. Further, upon the application of an electroforming potential the Ag^+ ions form an ionic filament which introduces a conductive pathway for transport of charge carriers. As such, the van der Waal spacing of InSe, the presence of selenium and indium vacancy defects from mechanical

exfoliation [17] along with the migration of mobile indium ions[22] allow the diffusion of silver into the InSe to form a conductive pathway that induces non-volatile switching in InSe memory cell.

To further investigate the mechanism facilitating the migration of Ag^+ ions in our InSe memory device, theoretical modelling of the diffusion of Ag and *oxygen* (O) atoms through a representative γ-InSe structure is carried out. For this, we calculated the diffusion energy barrier using DFT as described in the Supplementary Information, *Section 4*. The energy barrier is calculated as a function of the position of the Ag/O atom as it traverses along the *c*-axis of the structure, as displayed in **Figure 4a**. The direction of diffusion, starting and end position of the Ag/O atom has been shown by an arrow. The application of an electric field perpendicular to the sample will force the oxygen *ion* (O^{2-}) and Ag^+ ions to migrate in opposite directions due to their opposite charges, where the movement of the Ag or O atoms can be forwards or backwards according to the start and end points. The relative energy of the supercell as a function of the vertical position of the Ag/O atom is depicted in Figure 4b. The barrier for diffusion of the O atom is calculated to be ~3.7 eV which is larger than for diffusion barrier of Ag calculated to be ~2.3 eV. This suggests that the diffusion of Ag is likely to be preferred over

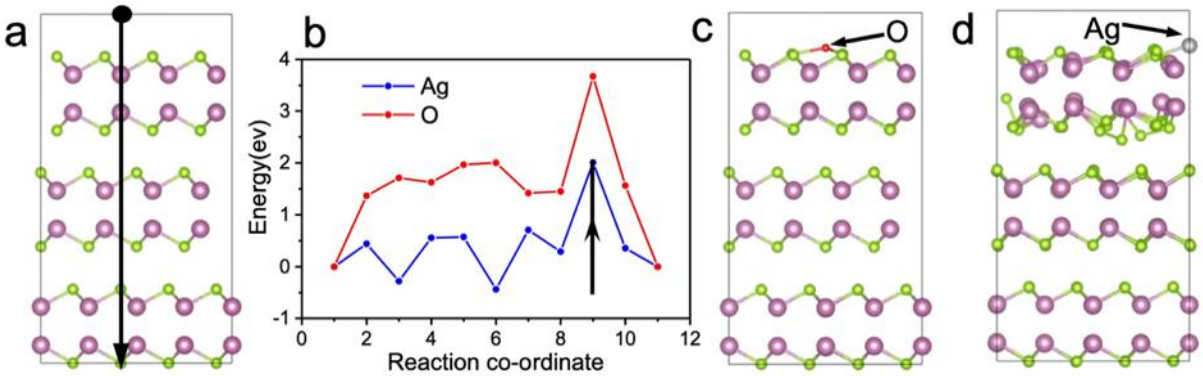

Figure 4: DFT calculations for diffusion energy barrier in InSe memory cell. The (a) side view of the bulk γ-InSe structure, showing the start and end point of the Ag/O atom (shown as a black sphere) along the diffusion pathway. In the shown InSe trilayer structure the Indium and Selenium atoms are indicated by purple and green colour respectively. (b) The total system energy as a function of the reaction coordinate, which is the position of the Ag atom and the O atom. The structure of the γ-InSe when the (c) O atom and the (d) Ag atom occupies the position indicated by an arrow in Figure (b).

that of O under the applied electric field along the *c*-axis which is consistent with our experimental observation (as discussed in cross-sectional TEM analysis, Figure 3). *To understand the diffusion dynamics, both anion-anion repulsion between O and selenium (Se) and cation-cation repulsion between indium (In) and Ag were considered. We have confirmed that the O-Se repulsion is higher than that of Ag-In by performing a partial charge calculation using the Bader charge analysis.*[52] *The calculated partial charges for In, Ag, Se and O are +0.6|e|, +0.2|e|, -0.6|e| and -1.0|e|, respectively. The product of the cationic charges is one-fifth of that of the anionic charges, confirming our statement on the relatively larger anion-anion repulsion. This* resistance to O diffusion might be driven by the *high* anion-anion repulsion between oxygen (O^-) and selenium (Se^-) ions, as can be seen in Figure 4c. In the structure shown, the O atom is at a position that is close to the Se atoms, and even though the structure does not sustain significant forces (as it is a high-energy structure) and is in fact the structure that corresponds to the highest energy along the reaction coordinate. In the case of Ag (Figure 4d), the structure displayed also corresponds to the point of highest energy barrier in Figure 4b (indicated by an arrow), but the resistance to diffusion in this case is caused by

the significant structural change due to the presence of the Ag atom at the corresponding position along the reaction coordinate. These results are in alignment with the experimental observations, further validating our hypothesis.

Conclusion

In summary, we report a non-volatile layered InSe based memory cell. The charge transport mechanism in the device relies on the diffusion of silver ions through the InSe stack. The presence of vacancy defects from the fabrication processes and the presence of van der Waals spacing allows for the reversible and repeatable traversal of the ions under an applied electric field. DFT calculations and experimental elemental analysis are used to validate and support the mechanism of silver ion diffusion in InSe for filamentary conduction. The memory cell exhibits high switching ratios ($>10^3$) with long retention periods ($>10^5$ s), demonstrating the viability of InSe in the next generation of memory and neuromorphic computing technology.

4. Experimental Methods

Device Fabrication

Using standard photolithography, electron beam assisted metal deposition and lift-off process, 25 nm Ag with a 5 nm Ti adhesion layer were fabricated as bottom electrodes on SiO_2 (300 nm)/Si substrates. Bulk InSe crystals (purchased from 2D Semiconductors) are mechanically exfoliated onto

polycarbonate films. Exfoliated flakes of interest were optically identified and transferred onto the bottom Ag electrodes using a HQ Graphene+ manual transfer stage. After the transfer, the polycarbonate film was dissolved in chloroform. Subsequently, another round of photolithography, electron beam assisted metal deposition and lift-off process, was carried out to realize the top Au electrode of 100 nm with a Cr adhesion layer of 10 nm. Based on the lateral dimension on the transferred InSe multiple crossbar devices with active area of 4×2 μm^2 and 4×4 μm^2 were fabricated.

Electrical Characterization

All electrical characterizations were done on the crossbar devices using a Keithley 4200SCS-A parameter analyser. Measurements were carried out in ambient conditions while biasing the bottom Ag electrode with the top Au electrode being grounded.

Material Characterization

PL and Raman spectroscopy was carried out on a Horiba LabRam Raman setup, equipped with a 532 nm laser as an excitation source. An 1800 grooves/mm grating was used for the Raman shift characterization and a 600 grooves/mm grating for PL characterization.

Thicknesses of the transferred InSe flakes were determined by using a Bruker AFM, working in ScanAsyst and TespaV2 modes. TEM analysis was performed by preparing a lamella using a Dual Beam Focused ion beam (FIB) on a JEOL F200 TEM operating at 200 kV, equipped with a cold field emission gun (CFEG). EDX was performed using an Oxford X-Max^n 80T detector.

Acknowledgements:

This work was performed in MNRF facility in RMIT university in the Victorian Node of the Australian National Fabrication Facility (ANFF) and the RMIT Microscopy and Microanalysis Research Facility (RMMF). SPR acknowledges the support of the Australian Government through the Australian Research Council (ARC) under the Centre of Excellence scheme (project number CE170100026). This work was also supported by computational resources provided by the Australian Government through the National Computational Infrastructure National Facility.

References

[1] W. Sun, B. Gao, M. Chi, Q. Xia, J. J. Yang, H. Qian, H. Wu, *Nature communications* **2019**, 10, 1.

[2] Z. Wang, S. Joshi, S. Savel'ev, W. Song, R. Midya, Y. Li, M. Rao, P. Yan, S. Asapu, Y. Zhuo, *Nature Electronics* **2018**, 1, 137.

[3] M. A. Zidan, Y. Jeong, J. Lee, B. Chen, S. Huang, M. J. Kushner, W. D. Lu, *Nature Electronics* **2018**, 1, 411.

[4] F. Rahman, T. Ahmed, S. Walia, E. Mayes, S. Sriram, M. Bhaskaran, S. Balendhran, *Nanoscale* **2018**, 10, 19711.

[5] L. Zhang, T. Gong, H. Wang, Z. Guo, H. Zhang, *Nanoscale* **2019**, 11, 12413.

[6] T. Ahmed, S. Walia, E. L. Mayes, R. Ramanathan, V. Bansal, M. Bhaskaran, S. Sriram, O. Kavehei, *Scientific reports* **2019**, 9, 1.

[7] D. Ham, H. Park, S. Hwang, K. Kim, *Nature Electronics* **2021**, 4, 635.

[8] S. Lv, J. Liu, Z. Geng, *Advanced Intelligent Systems* **2021**, 3, 2000127.

[9] Y. Liu, X. Duan, Y. Huang, X. Duan, *Chemical Society Reviews* **2018**, 47, 6388.

[10] X. Feng, Y. Li, L. Wang, S. Chen, Z. G. Yu, W. C. Tan, N. Macadam, G. Hu, L. Huang, L. Chen, *Advanced Electronic Materials* **2019**, 5, 1900740.

[11] H. Zhao, Z. Dong, H. Tian, D. DiMarzi, M. G. Han, L. Zhang, X. Yan, F. Liu, L. Shen, S. J. Han, *Advanced Materials* **2017**, 29, 1703232.

[12] Y. Wang, F. Wu, X. Liu, J. Lin, J.-Y. Chen, W.-W. Wu, J. Wei, Y. Liu, Q. Liu, L. Liao, *Applied Physics Letters* **2019**, 115, 193503.

[13] X. Yan, Q. Zhao, A. P. Chen, J. Zhao, Z. Zhou, J. Wang, H. Wang, L. Zhang, X. Li, Z. Xiao, *Small* **2019**, 15, 1901423.

[14] L. Liu, Y. Li, X. Huang, J. Chen, Z. Yang, K. H. Xue, M. Xu, H. Chen, P. Zhou, X. Miao, *Advanced Science* **2021**, 2005038.

[15] M. Wang, S. Cai, C. Pan, C. Wang, X. Lian, Y. Zhuo, K. Xu, T. Cao, X. Pan, B. Wang, *Nature Electronics* **2018**, 1, 130.

[16] M. R. Molas, A. V. Tyurnina, V. Zólyomi, A. K. Ott, D. J. Terry, M. J. Hamer, C. Yelgel, A. Babiński, A. G. Nasibulin, A. C. Ferrari, *Faraday Discussions* **2021**, 227, 163.

[17] L. Shi, Q. Zhou, Y. Zhao, Y. Ouyang, C. Ling, Q. Li, J. Wang, *The journal of physical chemistry letters* **2017**, 8, 4368.

[18] A. A. Kistanov, Y. Cai, K. Zhou, S. V. Dmitriev, Y.-W. Zhang, *Journal of Materials Chemistry C* **2018**, 6, 518.

[19] Y.-R. Chang, P.-H. Ho, C.-Y. Wen, T.-P. Chen, S.-S. Li, J.-Y. Wang, M.-K. Li, C.-A. Tsai, R. Sankar, W.-H. Wang, *ACS Photonics* **2017**, 4, 2930.

[20] S. Lei, F. Wen, L. Ge, S. Najmaei, A. George, Y. Gong, W. Gao, Z. Jin, B. Li, J. Lou, *Nano letters* **2015**, 15, 3048.

[21] Q. Zhao, W. Wang, F. Carrascoso-Plana, W. Jie, T. Wang, A. Castellanos-Gomez, R. Frisenda, *Materials Horizons* **2020**, 7, 252.

[22] M. Mathew, R. Jayakrishnan, P. Ratheesh Kumar, C. Sudha Kartha, K. Vijayakumar, Y. Kashiwaba, T. Abe, *Journal of applied physics* **2006**, 100, 033504.

[23] M. Lübben, I. Valov, *Advanced Electronic Materials* **2019**, 5, 1800933.

[24] D. S. Jeong, C. S. Hwang, *Advanced Materials* **2018**, 30, 1704729.

[25] Q. Tian, X. Zhang, X. Zhao, Z. Wang, Y. Lin, H. Xu, Y. Liu, *IEEE Electron Device Letters* **2020**, 42, 308.

[26] H. Abbas, A. Ali, J. Jung, Q. Hu, M. R. Park, H. H. Lee, T.-S. Yoon, C. J. Kang, *Applied Physics Letters* **2019**, 114, 093503.

[27] Y. Kim, H. Choi, H. S. Park, M. S. Kang, K.-Y. Shin, S.-S. Lee, J. H. Park, *ACS applied materials & interfaces* **2017**, 9, 38643.

[28] S. R. Tamalampudi, Y.-Y. Lu, R. K. U, R. Sankar, C.-D. Liao, C.-H. Cheng, F. C. Chou, Y.-T. Chen, *Nano letters* **2014**, 14, 2800.

[29] Z. Li, H. Qiao, Z. Guo, X. Ren, Z. Huang, X. Qi, S. C. Dhanabalan, J. S. Ponraj, D. Zhang, J. Li, *Advanced Functional Materials* **2018**, 28, 1705237.

[30] M. Dai, H. Chen, F. Wang, Y. Hu, S. Wei, J. Zhang, Z. Wang, T. Zhai, P. Hu, *ACS nano* **2019**, 13, 7291.

[31] L. Guo, B. Mu, M.-Z. Li, B. Yang, R.-S. Chen, G. Ding, K. Zhou, Y. Liu, C.-C. Kuo, S.-T. Han, *ACS Applied Materials & Interfaces* **2021**, 13, 39595.

[32] J. Shang, L. Pan, X. Wang, J. Li, Z. Wei, *Semiconductor Science and Technology* **2018**, 33, 034002.

[33] Q. Hao, J. Liu, G. Wang, J. Chen, H. Gan, J. Zhu, Y. Ke, Y. Chai, J. Lin, W. Zhang, *ACS nano* **2020**, 14, 11373.

[34] T. Zheng, Z. Wu, H. Nan, Y. Yu, A. Zafar, Z. Yan, J. Lu, Z. Ni, *RSC advances* **2017**, 7, 54964.

[35] M. Wu, Q. Xie, Y. Wu, J. Zheng, W. Wang, L. He, X. Wu, B. Lv, *Aip Advances* **2019**, 9, 025013.

[36] A. S. Nissimagoudar, J. Ma, Y. Chen, W. Li, *Journal of Physics: Condensed Matter* **2017**, 29, 335702.

[37] S. Liu, N. Lu, X. Zhao, H. Xu, W. Banerjee, H. Lv, S. Long, Q. Li, Q. Liu, M. Liu, *Advanced Materials* **2016**, 28, 10623.

[38] A. Wedig, M. Luebben, D.-Y. Cho, M. Moors, K. Skaja, V. Rana, T. Hasegawa, K. K. Adepalli, B. Yildiz, R. Waser, *Nature nanotechnology* **2016**, 11, 67.

[39] K. M. Kim, J. J. Yang, J. P. Strachan, E. M. Grafals, N. Ge, N. D. Melendez, Z. Li, R. S. Williams, *Scientific reports* **2016**, 6, 1.

[40] B. Shi, Y. Wang, J. Li, X. Zhang, J. Yan, S. Liu, J. Yang, Y. Pan, H. Zhang, J. Yang, *Physical Chemistry Chemical Physics* **2018**, 20, 24641.

[41] Z. Lv, Q. Hu, Z. X. Xu, J. Wang, Z. Chen, Y. Wang, M. Chen, K. Zhou, Y. Zhou, S. T. Han, *Advanced Electronic Materials* **2019**, 5, 1800793.

[42] D. G. Hopkinson, V. Zólyomi, A. P. Rooney, N. Clark, D. J. Terry, M. Hamer, D. J. Lewis, C. S. Allen, A. I. Kirkland, Y. Andreev, *ACS nano* **2019**, 13, 5112.

[43] H. Wang, J.-j. Shi, P. Huang, Y.-m. Ding, M. Wu, Y.-l. Cen, T. Yu, *Physica E: Low-dimensional Systems and Nanostructures* **2018**, 98, 66.

[44] H. Arora, A. Erbe, *InfoMat* **2021**, 3, 662.

[45] X. Wei, C. Dong, A. Xu, X. Li, *Applied Surface Science* **2019**, 475, 487.

[46] K. Xiao, A. Carvalho, A. C. Neto, *Physical Review B* **2017**, 96, 054112.

[47] S.-w. Chen, J.-s. Chang, S.-m. Tseng, L.-c. Chang, J.-y. Lin, *Journal of Alloys and Compounds* **2016**, 656, 58.

[48] Y. Yang, P. Gao, S. Gaba, T. Chang, X. Pan, W. Lu, *Nature communications* **2012**, 3, 1.

[49] F.-S. Yang, M. Li, M.-P. Lee, I.-Y. Ho, J.-Y. Chen, H. Ling, Y. Li, J.-K. Chang, S.-H. Yang, Y.-M. Chang, *Nature communications* **2020**, 11, 1.

[50] A. Matikainen, T. Nuutinen, T. Itkonen, S. Heinilehto, J. Puustinen, J. Hiltunen, J. Lappalainen, P. Karioja, P. Vahimaa, *Scientific reports* **2016**, 6, 1.

[51] K. Ranganathan, M. Fiegenbaum-Raz, A. Ismach, *Advanced Functional Materials* **2020**, 30, 2005718.

[52] W. Tang, E. Sanville, G. Henkelman, *Journal of Physics: Condensed Matter* **2009**, 21, 084204.

Atomically thin 2D materials are increasingly being investigated for their resistive switching properties. Understanding preferential ion diffusion can pave the way for high performance, tailored non-volatile memory technology based on such material systems. Electrical and microscopic characterization along with theoretical modelling of InSe reveals the material specific preferential diffusion of cations/anions for high-performance filamentary switching in 2D materials.